

The Shear and Axial Load Behaviour of Seismic Isolation Bearings

A.J. Carr¹, N. Cooke¹, A. Mori² and P.J. Moss¹

SUMMARY

The experimental work covering a range of different sizes and hardnesses of seismic isolation bearings, considering both laminated elastomeric and lead-rubber bearings, was undertaken to investigate the stress distributions normal to the bearing faces as the shearing deformation was increased. The normal stress distributions show the degree of the bearing stability and illustrate a distinct difference between a well confined load state and a poorly confined loading state of the bearings. Analytical investigations using the finite element method were carried out to verify the experimental bearing behaviour and to investigate the interaction between the rubber and steel shim layers in the bearings.

INTRODUCTION

A large number of seismic isolation systems have been developed since the early 1970's. They are basically a combination of elastomeric bearings and energy dissipators such as lead-plugs, steel bars, steel springs, steel plate, and a combination of sliding bearings and re-centering devices. However, most of the studies on seismic-isolation systems have been related to energy dissipators, sliding bearings or the seismic-isolation itself. Elastomeric bearings play an important part in seismic isolation systems since they can lengthen the period of free vibration of a structure. The properties of elastomeric bearings have been investigated since 1940 in applications as bridge bearings and the existing design codes for elastomeric bearings are based on that research. This previous research work concerned the support of the dead and live loads by the compressive behaviour of the bearings, the understanding of the expansion and contraction of bridge decks due to temperature variations, and how these affect the lateral behaviour of bearings. The results of this research have been used also for the design of elastomeric bearings that form part of a seismic-isolation system. It seemed desirable therefore to investigate the current code requirements [AASHTO (1989); Austr. Std 1523 (1981); Br. Std 5400 (1983); High. Dir., D.O.E., Gt Br. (1976); Min. of Constr., Japan (1991); M.W.D., NZ (1981a,b)] when the performance of the elastomeric bearings is examined as part of a seismic resistance system.

The experimental work described here and in the references by Mori [1993] and Mori et al [1995a,b] was undertaken for both laminated elastomeric bearings (EB) and lead-rubber bearings (LRB) to obtain a better understanding of the real bearing behaviour under different types of deformation such as compression, shear and rotation. In particular, the investigation focused on the distributions of vertical pressure (normal stress) on the bearing faces and the degree of lift-off of the edges of the bearings as

¹ University of Canterbury, Christchurch, New Zealand

² Japan Engineering Consultants Ltd, Tokyo, Japan

the shearing displacement and the angle of rotation increased.

The force-displacement response and normal stress distribution of the bearings in shear and rotation were determined by testing pairs of bearings in a specially developed self-equilibrating test frame using an Avery 1000 kN testing machine to apply an axial load and a double acting hydraulic jack to apply the shearing forces.

EXPERIMENTAL INVESTIGATION

Five elastomeric bearing pairs and two lead-rubber bearing pairs were tested in the experimental program. Each pair was produced from the same batch of natural rubber and it was assumed that they would have identical properties. The principal plan dimensions of the selected bearings were 380 mm x 300 mm, with heights of 130 mm to 148 mm (see Table 1). The dimensions were similar to those normally used for bridge bearings in New Zealand and were the maximum dimensions that could be accommodated by the axial loading machine.

Table 1 Properties and Construction of the Bearings Tested

Bearing No.	1	2	3	5	6	7	8
Hardness degree for rubber	53	48	57	53	53	48	48
Construction							
no. of rubber inner layers	9	10	9	9	9	9	9
no. of steel shims (3 mm) ¹	10	10	8	8	8	8	8
no. of 10 mm outer steel plates ¹	-	1	2	2	2	2	2
size of lead plug (mm)	-	-	-	-	75	-	75
outer rubber thickness (mm)	5	4	5	5	5	5	5
side rubber cover thickness (mm)	7	10	10	10	10	10	10
total rubber thickness (mm)	100	108	100	100	100	100	100
total height of bearing (mm)	130	148	144	144	144	144	144
Shape factor							
inner layer	6.6	7.9	7.9	7.9		7.9	
outer layer	9.4	14.1	11.3	11.3		11.3	
Calculated stiffness ²							
compression (kN/mm)	125	170	258	222	-	182	-
shear (kN/mm)	0.72	0.68	1.14	0.93	8.58 ³ 1.32 ⁴	0.76	7.05 ³ 1.08 ⁴
Applied maximum axial load (kN)	450	650	800	800	800	650	650

Note: 1) mild steel (Grade 250)

2) determined from BE1/76 [1976] for EB and CDP818/A [1981a] for LRB

3) initial stiffness of the lead rubber bearing

4) post-elastic stiffness of the lead rubber bearing

The EB consisted of alternating 10 mm thick rubber inner layers and 3 mm thick steel shims with 10 mm thick steel outer plates and 5 mm thick rubber top and bottom cover layers. The LRB were of similar construction but with lead plugs of 75 mm diameter set into the centre of the bearing. The construction and properties of the bearings tested is summarised in Table 1. The bearing number 1, B1,

was used for pretesting and to investigate the effect of plan dimension variation, these being 432 mm x 205 mm.

The design of EB was based on the British Dept of the Environment Memorandum BE1/76 [1976] and the design of the LRB on the New Zealand Ministry of Works and Development (MWD) CDP 818/A [1981a]. The shape factors in Table 1 were calculated for the inner layers using the formula

$$\text{Shape factor, } S = \frac{L_e W_e}{2t_e (L_e + W_e)} \quad (1)$$

where L_e and W_e are the length and width respectively of the inner steel shims and t_e is the thickness of a rubber layer. For the outer layers, the equation in BE1/76 was used (the effective rubber thickness is estimated as 1.4 times the actual rubber thickness), i.e.

$$\text{Shape factor, } S = \frac{L_e W_e}{2.8t (L_e + W_e)} \quad (2)$$

Test Rig and Instrumentation

As shown in Figure 1, a self-equilibrating frame was used to test a "back-to-back" double-bearing system in shear.

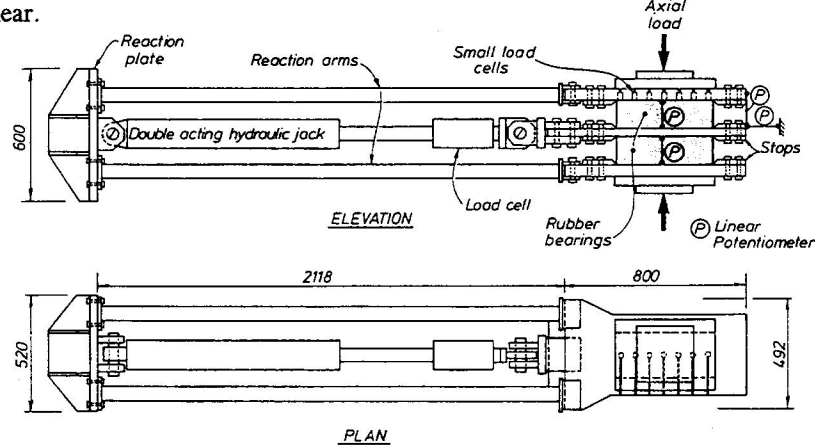


Figure 1 Test rig used for the shear tests

An Avery 1000 kN capacity test machine was used to apply the axial loads and a double acting hydraulic jack applied the static cycling shearing forces via a load cell. The top and bottom platens of the axial loading machine were very rigid and the vertical movement of the system could be neglected. The hydraulic jack was connected to the centre plate and the reaction plate by pins at each end.

The pin connections at the ends of the hydraulic jack were set to follow the natural deformation of the bearings during the shear tests. The reaction arms were designed to be sufficiently flexible that bending moments were minimised when the bearings were compressed and the shearing deformation increased.

Two linear potentiometers for each bearing were centrally placed on both sides of the bearings to measure vertical deformations. One linear potentiometer was located at the back of the top bearing to measure the vertical displacement so that the angle of rotation of the bearings due to the shearing force might be calculated. Two large linear potentiometers were fixed to the centre plate and were used to measure the relative shearing displacement of the bearings.

Stops constructed from pieces of steel plates with one chamfered edge at the face next to the bearings were bolted onto the loading plates in order to avoid slippage of the bearings on the loading plates. The outer rubber layers and outer steel plates of the bearings were constrained by these stops. Some codes recommend the use of dowels to retain bearings in position or to transmit shear forces. However, in situations where bearings need replacement, the use of dowels has made removal of the bearings difficult. Moreover, if dowels had been used in this test programme, their presence in the face of the bearing would have made it difficult to measure the vertical pressure distribution using the small load cells used for this purpose.

Small Load Cells (SLC)

A small load cell (SLC) consisting of a hollow cylinder 30 mm high and 20 mm diameter having a minimum wall thickness of 0.6 mm made from a high strength (800 MPa) steel was developed specially to measure the normal stress distribution on the top and bottom faces of the bearings.

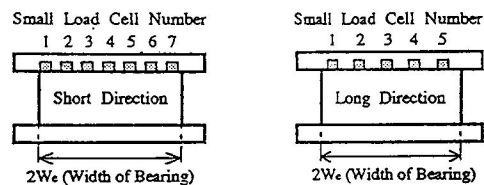


Figure 2 Configuration of the SLCs in the short and long directions of bearing

The location of the small load cells in the short and long directions is shown in Figure 2. The performance of the SLC was verified by examining the test results in terms of the vertical stress across Bearing 2 under an axial load of 650 kN [Mori (1993), Mori et al (1995a)]. It was found that the performance of the SLCs was reasonably reliable in terms of both the calculated reaction force and the shape of the measured normal stress distribution and the axial compression load.

General trend of the stress distribution for EBs

Figure 3 shows the stress distributions across the bearing top face of Bearing 7 in the short direction as the bearing shear strain increases from 0% to 150% for a compressive load of 440 kN and from 0% to 200% for an compressive load of 650 kN. It can be seen from bearing shear strain in the figure that the contact condition between the SLCs and the face of the bearing does not seem good for the low compressive load probably due to an inadequate amount of compressive load on the bearings. When the bearing shear strain reached about 125%, the normal stress at the bearing centre (SLC No. 4) started to decrease. Beyond this bearing shear strain, the change of the normal stress distribution rapidly progressed and lift-off of the bearing at 200% bearing shear strain occurred for nearly 50% (half of the bearing width) of the contact area between the bearing faces and the loading plates. The maximum normal stress under only compressive load on the bearings is about twice the average compressive stress caused by the compressive load and it may reach about nearly four times the average compressive load at the bearing edges at 200% bearing shear strain if the effect of the stops at the bearing edges is taken into consideration [Mori et al (1995a)].

Normal stress distributions of well confined and poorly confined LRBs

The normal stress distribution across the top face of the LRB (Bearing 6) at 150% bearing shear strain under the design compressive load of 800 kN is shown in Figure 4 together with the normal stress distribution of the EB (Bearing 5) which has the same rubber hardness as the LRB.

As can be seen in the Figure, No. 3 SLC was placed on both the lead plug and the rubber faces. Therefore the normal stress of the LRB at the SLC No. 3 was higher than that of the EB due to the boundary discontinuity between the lead plug and the rubber on the surface of the LRB as the bearing shear strain increased or the deformation of the faces of the lead plug progressed and this value was not necessarily accurate. However since the normal stress distribution of the LRB at 0% bearing shear strain was similar to that of the EB [Mori (1993), Mori et al (1995a)], it was found that if the LRB was well confined by the appropriate compressive load, the normal stress distribution on the faces of the LRB could be generally regarded as the same as those of the EB even though the discontinuity due to the lead plug caused high local normal stresses at the boundary between the lead plug and the rubber in the LRB.

Figure 5 shows the normal stress distributions of the LRB (Bearing 6) at the various bearing shear strains under a low compressive load of 270 kN. Because the LRB was confined by an inappropriate compressive load, the lead plug carried very high normal stress, about 6 to 7 times the average compressive stress at 0% to 50% bearing shear strain and this was very different from that under the high compressive load. These normal stress distributions were also different from those of the EB, and the boundary discontinuity between the lead plug and the rubber had a marked effect on the normal stress distributions of the LRB.

Figures 6 and 7 show the hysteresis loops corresponding to the well confined LRB of Figure 4 and the poorly confined LRB of Figure 5 respectively. The difference between them can be seen and the hysteretic action under the low compressive load shows a somewhat poor behaviour especially at the unloading state when compared with that under the high compressive load. This is clearly evident that LRB needs adequate compressive load to provide the better confinement of the lead plug minimising the boundary discontinuity on the bearing face.

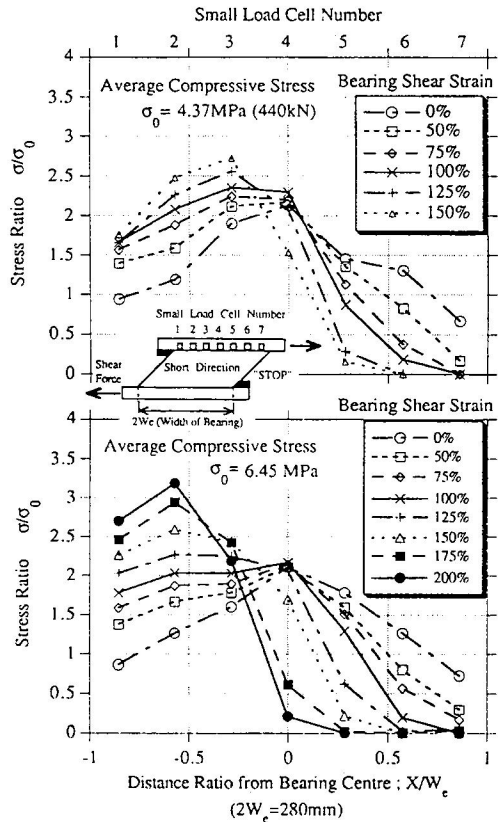


Figure 3 Normal stress distribution of an EB in the short direction as the bearing shear strain increases.

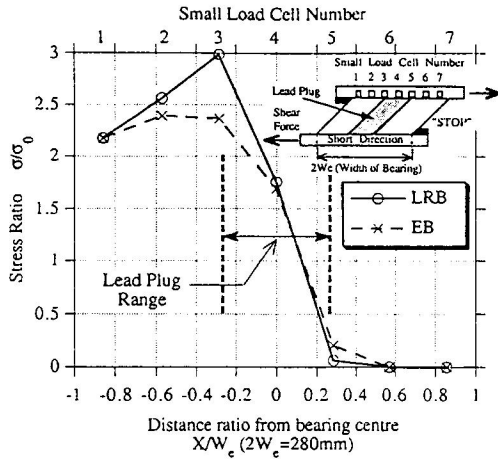


Figure 4 Normal stress distributions of a well confined LRB and EB at 150% bearing shear strain under the design compressive load.

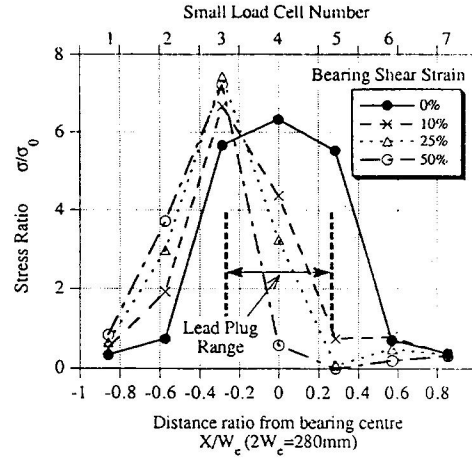


Figure 5 Normal stress distributions of a poorly confined LRB at the various bearing shear strain under a compressive load of 2701 kN.

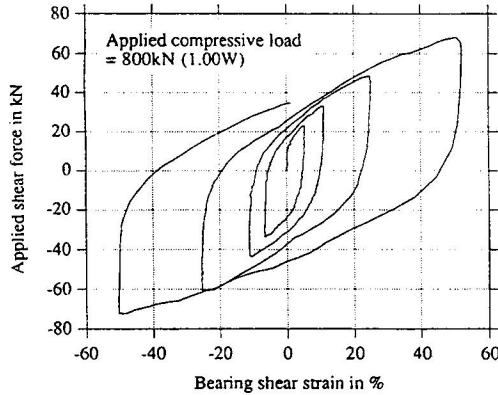


Figure 6 Hysteresis loop of a well confined LRB

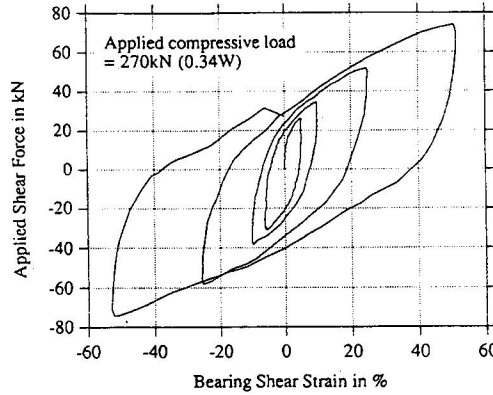


Figure 7 Hysteresis loop of a poorly confined LRB

ANALYTICAL INVESTIGATION

The finite element method was used to analytically investigate the behaviour of the seismic isolation bearings. Bearing 7 (EB) was dealt with in this study. In the finite element responses between the analysis and experiment analysis, the bearing was modelled by quadratic three dimensional solid elements. A rubber layer was modelled as two sub-layers to efficiently model the bulging deformation at the edges and a steel shim plate was modelled by a single layer of elements. The boundary between

the rubber layers and the steel shim plates was fixed as no bond failure was expected during the analysis from the observation of the experimental work. The top and bottom faces of the bearing were treated as frictional contact surfaces to model the real situation in the tests. The three dimensional model of half of the bearing is shown in Figure 8 using symmetry of the bearing and loading. The rubber was assumed to be an incompressible elastic material mathematically modelled by a strain energy functional form as fitting a second order polynomial using data from a rubber sample tested in tension. The steel was treated as a rate independent elasto-plastic material and its elastic modulus and Poisson's ratio were assumed to be 200 GPa and 0.27 respectively.

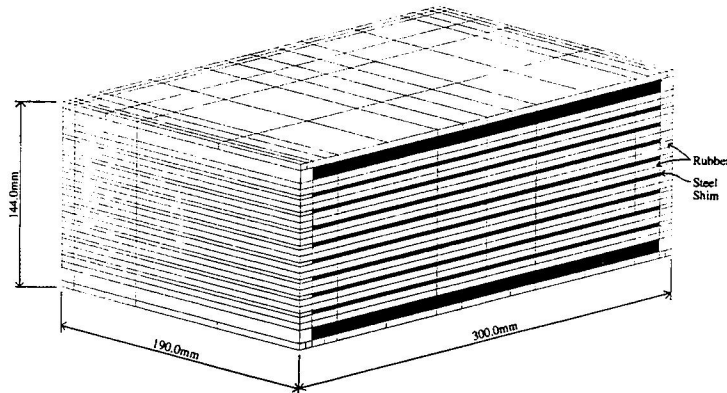


Figure 8 Elastomeric bearing model used in the analysis

Figure 9 shows the comparison of the shear force-deflection under the design compressive load. Figure 10 shows the comparison of the normal stresses between the analysis and the experiment at the bearing shear strains of 63% and 106% under the design compressive load. Both figures show that the analytical values of the above model are in a reasonably good agreement with the experimental values when the experimental errors due to the imperfections in the test rig are considered and it was concluded that the model used in this study showed a satisfactory degree of accuracy.

CONCLUSIONS

The following conclusions can be drawn from the investigations in this study.

1. The normal stresses across the bearing face measured by the small load cells clearly show the change of the bearing stability state.
2. It was observed that a well confined LRB showed similar normal stress distributions to the EB under the same loading conditions in spite of the presence of the lead plug.
3. Conversely, a poorly confined LRB showed a peculiar normal stress distribution as the lead plug carried most of the compressive load and the boundary discontinuity on the bearing face between the lead plug and rubber was marked.
4. The finite element analysis model helps to explain the behaviour of the bearing in terms of the force-deflection response and the normal stress distributions on the bearing face observed in the experiments.

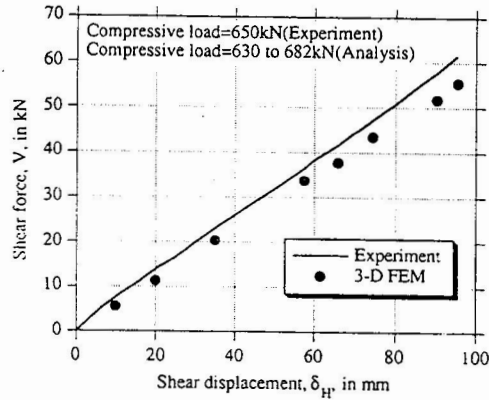


Figure 9 Comparison of the shear force - deflection response of an EB between the analysis and experiment in the short direction.

ACKNOWLEDGEMENT

The authors would like to thank Skellerup Industrial Ltd. in Christchurch, New Zealand for their cooperation of testing the rubber samples. The computer program used for the finite element analysis was "ABAQUS" (1991) under the licence from Hibbit, Karlsson and Sorensen Inc., USA.

REFERENCES

- AASHTO, *Standard Specifications for Highway Bridges*, 1989, 14th Edition, Washington DC, USA.
- Australian Standard, AS1523-1981, 1981, *Elastomeric Bearings for Use in Structures*.
- British Standard Institution, 1983, BS5400: *Steel, Concrete and Composite Bridges, Parts 9A and 9B*.
- Hibbit, Karlsson and Sorensen Inc. 1991. ABAQUS ver.4-9. USA.
- Highways Directorate, Dept of Environment, Great Britain, 1976, *Design Recommendations for Elastomeric Bridge Bearings*, Technical Memorandum BE1/76.
- Ministry of Construction, Japan, 1991, *Guidelines for Design of Base-Isolated Highway Bridges*, Tokyo.
- Ministry of Works and Development (MWD), New Zealand, 1981a, *Design of Lead-Rubber Bridge Bearings*, Civil Engineering Division, CDP 818/A., Wellington, NZ.
- Ministry of Works and Development, 1981b, *Elastomeric Bearing Specification 81/12/22/12*, NZ.
- Mori, A. 1993, *Investigation of the Behaviour of Seismic Isolation Systems for Bridges*, PhD Thesis, University of Canterbury, Christchurch, New Zealand.
- Mori, A, Carr, AJ, Cooke, N and Moss, PJ, 1995a, *The Compression Behaviour of Bearings Used for Seismic Isolation*, submitted to Engineering Structures.
- Mori, A, Carr, A J, Cooke, N and Moss, P J, 1995b, *The Behaviour of Bearings Used for Seismic Isolation Under Shear and Axial Load*, submitted to Earthquake Spectra.

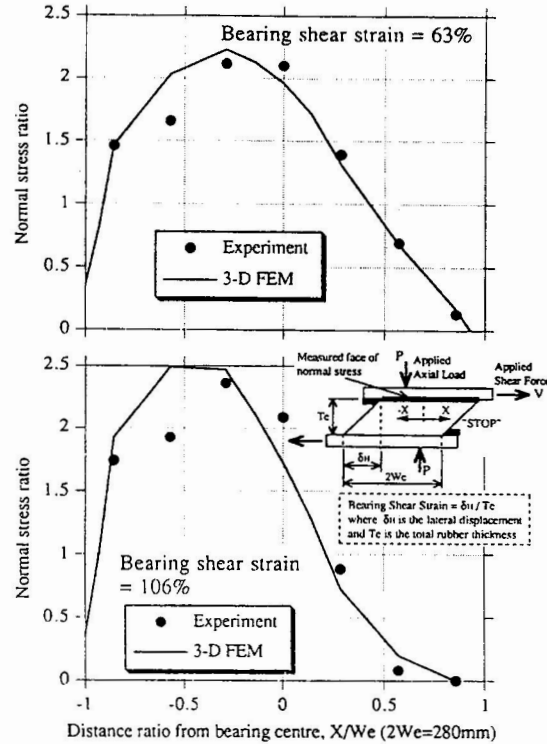


Figure 10 Comparison of the normal stresses of an EB between the analysis and experiment at the bearing shear strains of 63% and 106% under the design compressive load.